Pergamon

PII: S0191-8141(96)00035-1

Journal of Structural Geology, Vol. 18, No. 9, pp. 1127 to 1138, 1996

0191-8141/96 $15.00+0.00

An inverse method for determining three-dimensional fault geometry with thread criterion: application to strike-slip and thrust faults (Western Alps and California)

M. THIBAUT* and J. P. GRATIER

LGIT/CNRS-Observatoire, Université Joseph Fourier, IRIGM, BP 53X, 38041 Grenoble, France

M. LÉGER

Institut Français du Pétrole, Av. de Bois Préau, BP 311, 92506 Rueil-Malmaison, France

and

J. M. MORVAN

Département de mathématiques, Université Claude Bernard, 13-43 Bd du 11 novembre, 69621 Lyon, France

(*Received* 14 *July* 1995; *accepted in revised form* 12 *April* 1996)

Abstract—In order to draw geological structures such as faults, interpolation is generally needed between scattered data. The use of an approximation criterion integrating the kinematic properties of the faults helps to document the fault surfaces by adding a compatibility criterion to the data set. Assuming that two jointed blocks of rocks slipping on each other generate a thread surface, an approximation method has been developed which integrates a thread criterion. This approximation method is used to solve an inverse problem with least-squares criteria including proximity to data points, smoothness and thread criteria. The aim is to find a smooth surface which is as close as possible to a thread and as close as possible to the observed data set. Applications to two corrugated fault surfaces with a dense data set, located in the Western Alps (France) and in the Transverse Ranges (California), confirm the validity of the thread assumption. Despite their difference in mean corrugation wavelength (5 m and 10 km respectively), in the type of fault (strike-slip and thrust fault respectively), and in the nature of the faulted rocks (limestones and sandstones respectively), very similar results are obtained. In both cases the observed data fit well with a thread surface and the computed fault displacement fits well with the measured displacement on the fault (striae, seismic focal mechanism, geodetic data, restoration). The conclusion is that treating a fault as a thread is a valid physical description which gives the slip direction independently of other kinematic indicators. The advantage of using a thread criterion in addition to classical proximity and smoothness criteria is that this physical insight allows information from areas where data are relatively dense to help constrain areas where data are relatively sparse, these last areas being those that are usually not well constrained by proximity and smoothness criteria.

INTRODUCTION

When geological structures are drawn, the available data are generally so scattered that interpolation, or approximation, is needed between the observations.

Application of some simple rules including the restoration of structures (to their initial undeformed state) and the preservation of the rock volume before and after the deformation, adds some constraints to the geometry of the structures (Chamberlin 1910, Goguel 1952). For this purpose, balanced cross-section techniques have shown their efficiency within the plane strain basic assumption (Dahlstrom 1969, Hossack 1979, Suppe 1983).

For three-dimensional deformation several approaches have been used:

(a) Assuming simple fault and fold kinematics, for example when all the slip vectors for faults (Barr 1985) or flexural-slip folds (McCoss 1988), have parallel projections, three-dimensional restoration is possible. However, in this case the simplicity of the kinematics limits the application of the method.

(b) Assuming constant bed-length for the folded strata, several authors, such as Bennis *et al.* (1991), Lisle (1992) and Léger *et al.* (1995) proposed the use of appropriate geometrical properties: unfolding the developable surface without internal deformation means that the total curvature at any point of the surface (product of the two principal curvatures) is zero. This is efficient to test the geometry of folded strata. However, when considering folded and faulted strata, the geometry of the faults must be compatible with the geometry of the folded structures, and faults are not presumed to be developable surfaces.

(c) Restoration methods by best fitting of rigid blocks, (Cobbold 1979, Rouby *et al.* 1993) or by unfolding the folded structures, thus searching for the best fit between the unfolded blocks (Gratier *et al.* 1991, Gratier & Guillier 1993) can be used to test (by a trial and error approach) the geometrical compatibility of folded and faulted structures. However, this type of method only

*Also at: Institut Français du Pétrole, Av. de Bois Préau, BP 311, 92506 Rueil-Malmaison, France.

SG 18:9-B

tests the compatibility between the initial and the final state of the structures. With a constant bed length assumption, the geometry of pieces of strata (limited by faults) is tested by the compatibility of the geometry of hanging wall and foot wall traces on the faults, but such balanced finite geometries of folds and faults say nothing about the kinematics of the structures. When several layers are available, the kinematics are more constrained but are never fully integrated.

(d) In order to test the compatibility between folds and faults, Kerr *et al.* (1993) used inverse modelling where the geometry of two or more deformed layers is used to derive both the geometry of the main fault surface and the direction of extension. The assumption is that the deformation of the hanging wall is assumed to be an inclined shear deformation (with constant volume). Subject to the validity of this 'strong' kinematic assumption (which for example implies elongated strata), the finite geometry of the fault is known.

Following the idea that the use of an approximation criterion integrating the kinematic properties of the faults helps to document the fault surfaces (by adding a compatibility criterion to the data set), a new approach is proposed which is to solve an inverse problem when faults are assumed to be thread surfaces between jointed solid blocks. Thread surfaces have the characteristic property of being tangent to a non-zero twistor vector field, the field lines of this twistor being helices which may be compared with geological striae. The problem is illustrated in Fig. 1(a) showing that two jointed solid blocks slipping on each other generate a thread. Thread surfaces are the only surfaces allowing large displacement of two solid blocks which remain in contact during faulting. The most general example is the thread surface allowing movement between bolt and nut. However, in natural conditions, it is the slipping of one block against the other which generates the thread surface. In fact, most of the time, one of the blocks is more rigid than the other and the fault surface is located between one (relatively) rigid block and a gouge. It is important to emphasize that after a relatively large displacement, parallel to the fault, the fault surface must be smooth in the direction of slip (since the surface has been formed by the slipping) but the slip does not constrain the shape of the surface normal to the slip direction. Limitation of the thread assumption occurs if the fault geometry is modified by deformation (folding) either after the fault became inactive or during the time the fault is active. As the surrounding rocks must register such a deformation, careful structural analysis is always needed in the vicinity of the fault to estimate the kinematics of the deformation.

Natural fault surfaces are not perfect thread surfaces, firstly because of possible internal deformation of the blocks near the fault, and secondly because of the uncertainties of the data set. The best way to take into account these uncertainties is to use inverse methods with least-squares criteria. The aim of such a method is to find a smooth surface which is as close as possible to a thread and as close as possible to the observed data set. The

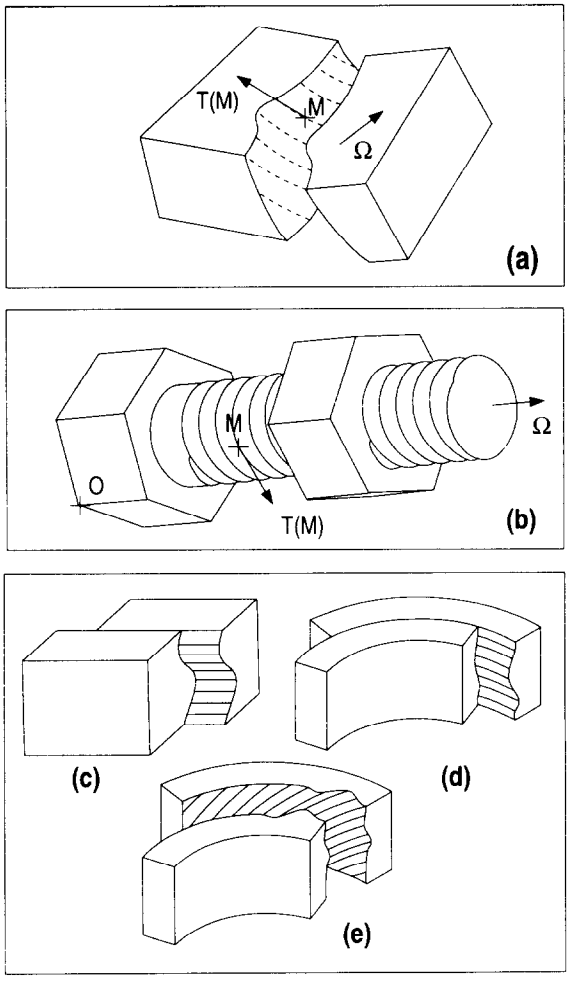

Fig. 1. (a) Two solid blocks slipping on each other generate a thread surface. The dashed lines represent the striae. ***M*** is a point on the thread surface. ***T(M)*** is the value of the twistor vector field at ***M***. **Ω** is the rotation vector of the twistor field. (b) The thread surface allows movement between bolt and nut. Examples of thread surfaces: (c) cylindrical surfaces (with straight striae), (d) surfaces of revolution (striae describe circles), (e) general case of a thread.

method is useful for constructing a fault surface from a set of scattered data points (fault position in boreholes, pickings on a seismic profile).

In order to test the effect of a thread criterion when interpolating scattered fault data, two types of approach have been compared (Thibaut 1994).

1. Starting from a geometrical approximation (which gives an intrinsic representation of the surface by minimizing criteria based on curvature and proximity to data points) a thread criterion is added and the two results (with and without a thread criterion) are compared in order to test the effect of the thread assumption. In this case the twistor is derived from the calculation and may be compared with geological striae.

2. Still starting from the same geometrical approximation, a thread criterion is added plus a given twistor (deduced from natural striae measurements, or from other information on the slip direction, such as seismic focal mechanisms). In this case, the results with and without a given twistor (in fact, with or without given slip direction) are compared.

Several questions arise from such an approach:

(a) can fault surfaces be considered as thread surfaces (in area of dense data)?

(b) does the use of a thread criterion improve the approximation of a fault surface (in areas with few data)?

(c) does the knowledge of the twistor (striae) help the approximation?

In the first instance, the inverse method is presented. Next an application to two different examples is presented: a decametric fault surface in the Western Alps (France) and a decakilometric fault surface in the Transverse Ranges, California (U.S.A.).

METHOD

The first problem is to represent a fault as a surface. Explicit representation associates a $z = f(x,y)$ coordinate (depth) to horizontal coordinates (x,y). However, vertical surfaces cannot be accurately described with such an explicit representation. Another way is to use parametric representation which means that each Cartesian coordinate (x, y, z) of the surface is associated with a couple (u,v) of curvilinear coordinates: $x = f(u,v)$, $y = g(u,v)$, $z = h(u,v)$. For numerical reasons these functions (f, g, h) must be discretized. Consequently, in order to ensure the smoothness of the surface, B-spline tensor products (third degree polynoms) were used to describe the surface (Schumaker 1981, Bartels *et al.* 1987).

Starting from an initial model of the surface, the inverse method involves making successive iterations in order to find the model of the fault surface which is as close as possible to the observed data. Each geometrical property (smoothness, thread) and geological information (location of fault points) is associated with a least-squares criterion which measures the discrepancy between computed data (model) and observed data (Tarantola 1987). The weighted sum (Q) of all the least-squares criteria is minimized with the Gauss–Newton algorithm. Starting from an initial model, the Q function is decreased at each iteration. The solution model is the model for which the derivative of Q (dQ) vanishes. The detailed mathematical method is described in Léger *et al.* (in press). Only a simplified description is given here for the geological application of the method.

$$Q = W_p Q_p + W_c Q_c + W_t Q_t + W_a Q_a + W_n Q_n. \quad (1)$$

The various least-squares criteria (Q_p, Q_c, Q_t, Q_a, Q_n) and weighting factors (W_p, W_c, W_t, W_a, W_n) are defined as follows: each least-squares criterion measures the discrepancy between computed data (with subscript c) and observed or known data (with subscript o).

Q_p measures the distance between each observed data item (P_o^i) and its homologue computed in the model fault surface (P_c^i). Q_p is a discrete sum because the data set is finite.

$$Q_p = \sum_i |P_o^i - P_c^i|^2. \quad (2)$$

Q_c measures the smoothness (or the regularity) of the surface. A surface is considered to meet the smoothness criterion if principal curvatures C_{c1} and C_{c2} are as close as possible to zero at any point. C_{o1} and C_{o2} are the observed curvatures assumed to be equal to zero. Since the criterion based on principal curvatures is defined as an integral instead of a discrete sum,

$$\begin{aligned} Q_c &= \int_S [(C_{c1} - C_{o1})^2 + (C_{c2} - C_{o2})^2] ds \\ &= \int_S (C_{c1}^2 + C_{c2}^2) ds \end{aligned} \quad (3)$$

with ds as the integration element of the surface.

Q_t represents the thread criterion. A thread surface is a regular surface tangent to a non-zero twistor. A twistor is a vector field with particular kinematic properties (Rougée 1982).

$$T(M) = \boldsymbol{T}(O) + \Omega \wedge \boldsymbol{OM}. \quad (4)$$

$T(M)$ is the value of the twistor vector field at any point M of the surface, OM denotes the vector linking point O to point M, Ω is a fixed vector which generates the axis of the thread, $T(O)$ is a constant vector at a fixed point O. In fact, $T(O)$ represents the translation component of the twistor, and Ω a rotation component for the twistor. As a typical example, a bolt and nut are in contact via a surface which is a thread. In this case (Fig. 1b), thread lines are helix lines (the field lines of the twistor). Particular instances of threads are cylindrical surfaces (helices degenerate into straight lines since their pitch becomes infinite, Fig. 1c), surfaces of revolution (helices become circles since their pitch is zero, Fig. 1d). Figure 1(e) illustrates the general case of a thread. Generating a thread surface by moving a curve along a non-zero twistor nowhere tangent to the curve may give a self-intersecting surface. In the following, however, we consider sufficiently small patches of threads that are non-self-intersecting surfaces. Because of this definition of a thread surface, the basic idea of a thread criterion consists of the minimization of the angle between the tangent plane and the twistor. Therefore, an objective function Q_t is defined as follows

$$Q_t = \int_S \langle \boldsymbol{T(M)}, \ \boldsymbol{N(M)} \rangle^2 ds. \quad (5)$$

Since $\boldsymbol{T(M)}$ is normalized, the dot product $\langle \boldsymbol{T(M)}, \boldsymbol{N(M)} \rangle$ represents the cosine of the angle between twistor $\boldsymbol{T(M)}$ at point M and plane $T_M S$ tangent at M to calculated surface S, with $N(M)$ being the unit vector normal to $T_M S$. Therefore, minimizing Q_t makes the surface and the twistor as tangential as possible, and hence the surface becomes as near as possible to a thread. The effects of this criterion on various theoretical examples are detailed in Léger *et al.* (in press).

Twistor T is *a priori* an auxiliary unknown which is determined at the same time as the surface. Sometimes, however, a particular twistor can be chosen on the basis of available geological information. For instance, if the

relative displacement of two blocks is known to be everywhere parallel to some unit vector T, the thread criterion simply makes the surface almost cylindrical with generatrices parallel to T.

The objective functions Q_a and Q_n have no geological meaning but are necessary for the inverse method (see Léger *et al* in press, for details).

Q_a is designed to solve the following problem. Since a given surface may be described by many parameterizations (a parameterization Φ maps some curvilinear coordinates (u,v) to Cartesian coordinates (x,y,z), $(x,y,z) = \Phi(u,v)$), the inverse problem may have many solutions in terms of parameterizations, even if it has only one solution in terms of surfaces. Therefore, an 'additional' criterion is introduced, which automatically selects the smoothest parameterization of a surface. This technique is presented in Rakotoarisoa (1992) and Léger *et al.* (1995).

Q_n solves the following problem. The thread criterion is perfectly met for any surface if twistor $\boldsymbol{T}$ is zero (vector $\boldsymbol{T(M)}$ is zero at any point M). This violates the definition of threads since the twistor should not be zero. Therefore, a 'normalization' criterion is introduced which makes the RMS (root mean square) norm of $\boldsymbol{T}$ over the surface close to one. Consequently, dot product $\langle \boldsymbol{T(M)}, \boldsymbol{N(M)} \rangle$ may be interpreted as an angle in a RMS sense since the norm of $\boldsymbol{N(M)}$ equals one. The expression of Q_n is

$$Q_n = \left| \int_S ||T(M)||^2 \mathrm{d}s - \int_S \mathrm{d}s \right|^2. \quad (6)$$

It is worth emphasizing that only the first three criteria (Q_p, Q_c, Q_t) have a geological meaning and a real effect on the solution.

With these last two criteria, the minimization of the overall weighted objective function Q is possible. However, weighted factors (W_c, W_p, W_t, W_a, W_n) are introduced in the Q calculation. This is done to give a degree of confidence to each criterion: proximity to the points, smoothness and thread. Greater or lesser importance may be given to each criterion with more or less weight. For example, for well data the location is very accurate and the weight for the proximity criterion may be very large. On the contrary, for seismic data (which are not so accurately located) this weight for the proximity criterion must be lowered.

For each geological application several tests have been run in order to compare different solution models with the following assumptions.

— Fault model without thread criterion: only the sum of the proximity (Q_p), smoothness (Q_c) and additional (Q_a) criterion has been minimized.

— Fault model with thread criterion and unknown twistor: the whole Q function has been minimized.

— Fault model with thread criterion and known twistor: the sum of the proximity (Q_p) smoothness (Q_c), thread (Q_t) and additional (Q_a) criteria has been minimized (since the twistor is known the Q_n function is not needed here). In this case the twistor is known from natural striae or seismic focal mechanisms.

In order to test the geological assumptions and to estimate the results of these comparisons, several residual criteria have been used.

The RMS distance is defined as the root mean square value of the distance between each data point (M_o) and its homologous data (M_c) on fault model

$$\text{RMS } \textit{distance} = \sqrt{((\sum_N (P_\perp(M_c^i - M_o^i))^2)/N)} \quad (7)$$

where N is the number of data points and $P_\perp$ denotes the normal projection to the surface.

To estimate how the fault model is close to a thread, an RMS angle is defined as follows.

$$\text{RMS } \textit{angle} = \sqrt{\int_S \langle \boldsymbol{T(M)}, \boldsymbol{N(M)} \rangle^2 \mathrm{d}s / \int_S \mathrm{d}s} \quad (8)$$

where $\langle \boldsymbol{T(M)}, \boldsymbol{N(M)} \rangle$ is the scalar product of the two vectors $\boldsymbol{T(M)}$ (twistor value at point M of the surface) and $\boldsymbol{N(M)}$ (the normal vector at point M of the surface). This RMS angle expresses how the twistor is tangent to the surface (or more exactly how it is perpendicular to the vector normal to this surface). As above, $\mathrm{d}s$ is the surface element.

APPLICATION TO THE STRIKE-SLIP CLÉRY FAULT (VERCORS, FRANCE)

The Cléry fault (Fig. 2) is a dextral strike-slip fault through the whole South Vercors massif (Robert 1976). The fault displacement is associated with the Alpine deformation (Gratier *et al.* 1989). The total horizontal offset on the Cléry fault and some other neighbouring parallel faults was first estimated to be about 3–4 km (Arnaud 1981) with the measurement of the offset of sedimentary units (southern limit of detrital limestones of the lower Barrémien). This value can be confirmed by measuring the difference in finite displacement between two cross-sections parallel to the fault (one north, the other south of the fault zone, Fig. 2b). Assuming a total duration of about 10 m.y. for this deformation, the mean slipping rate of the fault zone is about 0.4 mm/year. Small earthquakes are registered along this fault zone and along its north-east prolongation through the Belledonne massif. In detail, the fault zone is composed of several approximately parallel surfaces. Only one part of a single surface was measured. It is thus not easy to determine the true displacement on this particular fault element. The mechanism of sliding is mainly cataclastic sliding in contact with a gouge. The fault surface located in massive limestones is smooth, polished and reflective and this may indicate seismic sliding. Locally, aseismic creep markers (pressure solution cleavage) indicate that the whole displacement was partitioned between seismic and aseismic deformation. However, this process did not lead to significant mass transfer out of the studied fault surface.

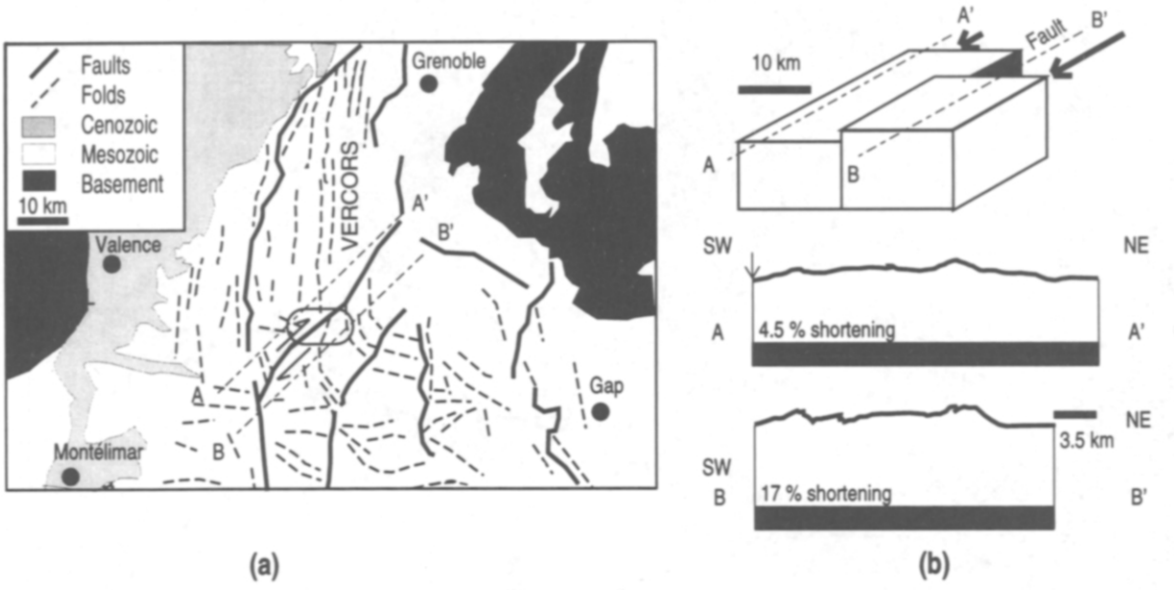

Fig. 2. (a) Structural map of the Chaînes Subalpines near the transition between Vercors and Diois: fold axes of different ages (Pyrénéo–Provencal and Alpine) and main thrust and strike-slip faults (after Gratier *et al.* 1989). (b) Cross-sections parallel to the Cléry fault zone. The shaded area is the basement. The thick lines are a reference folded layer (mid-Cretaceous). The total shortening parallel to the fault is different in the block north of the fault (4.5%) and in the block south of the fault (17%) indicating a relative displacement of about 3.5 km.

Data set: topographical survey

An element of the fault was surveyed with a theodolite and infrared distancemeter. One hundred and eight points of the fault surface were measured, the fault surface being defined as the surface with clear striae. The survey was linked to the national survey datum (IGN). Figure 3 gives a schematic view of the fault, Fig. 4 is the elevation of the fault along the y direction (see Fig. 3). These y values are the horizontal distance from a xz vertical reference plane parallel to the fault (strike 045°). The x axis is horizontal and parallel to the fault. The z axis is vertical and its origin is the 1860 m level (see legend of Fig. 4). The internal accuracy of the data set (concerning local coordinates xyz) is about 3 cm.

On the schematic diagram in Fig. 3, two types of surface are distinguished: shaded areas are fault surfaces (surfaces with clear striae) and white areas are outcrops which are not identified as fault surfaces. All fault surface outcrops are separated into two different fault surfaces: surfaces A and B. Only the surface A is discussed in detail here. Surface B is nearly flat and consequently tangent to several different twistors. Planes, spheres and cylinders of revolution have the common property to be tangent to several non-zero and non-parallel twistors.

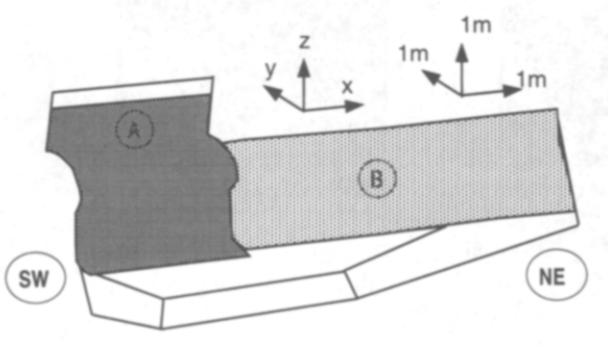

Fig. 3. Schematic diagram of the Cléry fault indicating the two surfaces studied (A and B). The shaded areas are the part of the outcrop which may be considered to be the fault surface (with striae). Area A corresponds to the left part of Fig. 4 (vertical axis numbers 2 to 6), area B corresponds to the right part of Fig. 4 (vertical axis numbers 6 to 12). The white area is the outcropping part which may have been partially destroyed by erosion.

Results

A preliminary model was run without imposing the striae. The results are given in Figs. 5 and 6. In Fig. 5, the contoured values are the y-values, whereas the vertical and horizontal axes are respectively the z and x axes (see Figs. 3 and 4). Crosses indicate the location of the surveyed data points. Figure 5(a) shows the fault model obtained without the thread criterion. Figure 5(b) shows the fault model obtained with the thread criterion, the surface and the twistor being simultaneously optimized. Comparison of Figs. 5(a) and (b) show that the difference between the two surfaces is rather small where the data points are dense. Figures 6(a) and (b) give the distance in cm between the calculated surface and the data points (trapezoidal boxes). Figure 6(b) shows in contours (labelled with rectangular boxes) the angle in degrees between the calculated surface and the associated optimal twistor. Figure 6(a) shows in contours the angle between the same twistor and the calculated surface displayed in Fig. 5(a). The RMS distance between the surface and the data points is 1.3 cm without the thread criterion and increases to 2.3 cm with the thread criterion, but both values are below the measurement uncertainties (3 cm). The RMS angle, which expresses the discrepancy from a perfect thread surface, is much lower with the thread criterion than without this criterion (Figs. 6a & b). With the thread criterion, and for the whole surface, the

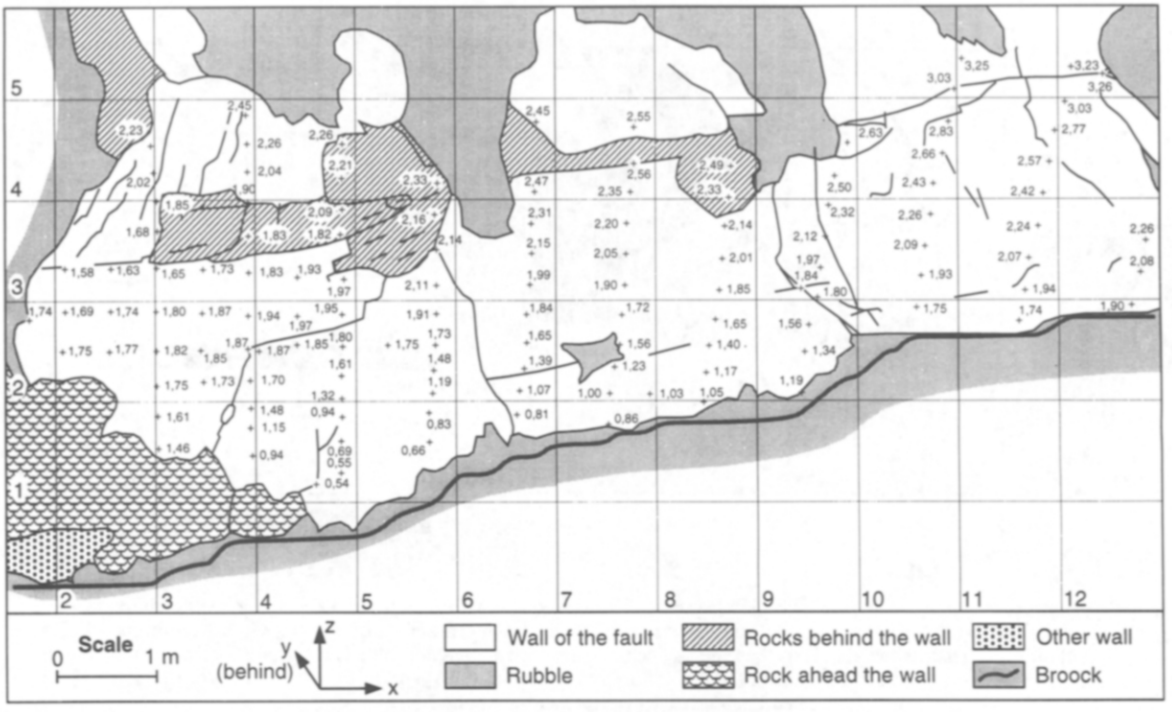

Fig. 4. Elevation of the fault surface surveyed with theodolite and infrared distancemeter, see Fig. 3. The y-values (digits on the map) are the horizontal distances from an xz vertical reference plane parallel to the mean fault plane (045°). The x axis is horizontal and parallel to the fault; along this x axis the unit element of the grid is 1 m in length. The origin of the vertical z axis is the 1860 m level. More precisely, the coordinates x, y, z of the marked points are related to Lambert coordinates XL, YL, ZL (zone III, France) according to the following equations: $x = (A + B)/1.414$, $y = (-A + B)/1.414$, $z = ZL - 1860$, with $A = XL - 851171$, $B = YL - 3287367$. Cléry fault, Chaînes Subalpines (Vercors), French Alps.

RMS angle value between the twistor and the tangential plane of the surface is about 1° instead of 8° without the thread criterion. It is interesting to note that this very low residual angle is obtained without a significant increase in the RMS distance, indicating that the modelled surface of the fault is very close to a perfect thread surface. This validates the assumption of a thread surface to model this natural fault surface. In the zone with local lack of data the introduction of the thread criterion modifies the surface geometry (see the change in contour lines near the lower-left part of the surface, Figs. 5a and b). Without the thread criterion, the effect of the Q_c minimization is to minimize the curvature. On the contrary, the thread criterion tends to document the whole surface using the

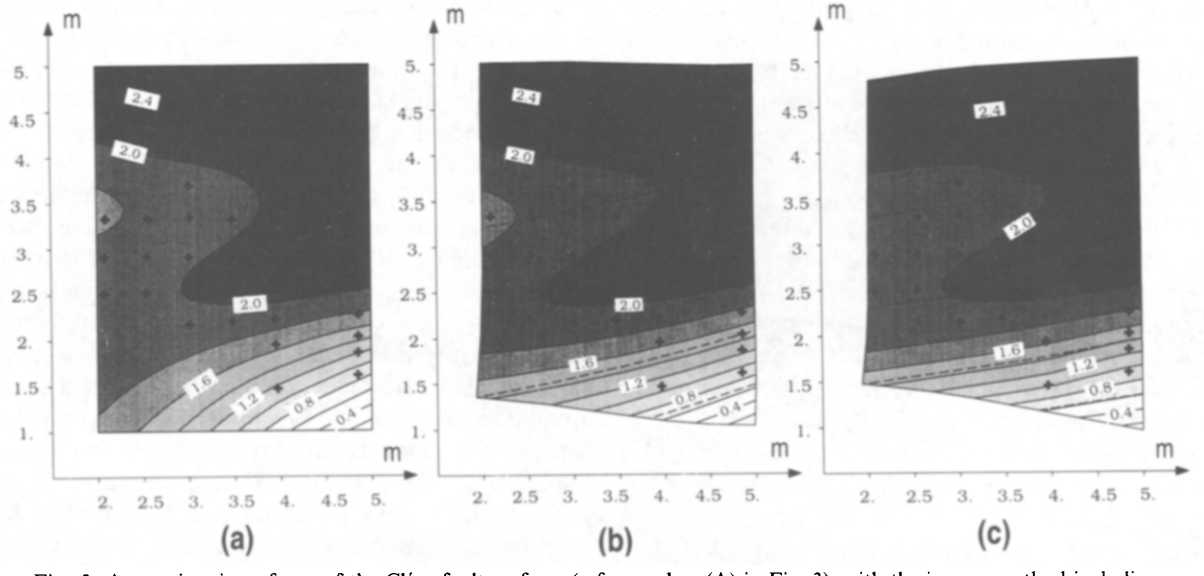

Fig. 5. Approximation of one of the Cléry fault surfaces (referenced as (A) in Fig. 3), with the inverse method including various least-squares criteria. (a) Approximation with proximity to data points and smoothness criteria. (b) Approximation with proximity to data points, smoothness and thread criteria. (c) Approximation with proximity to data points, smoothness, thread criteria and imposed striae. The contoured values are the y-values given in Figs. 3 and 4, the vertical and horizontal axes are respectively the z and x axes of Figs. 3 and 4. Crosses indicate the location of the surveyed data points on the fault surface. Dashed lines show the calculated twistor vector field.

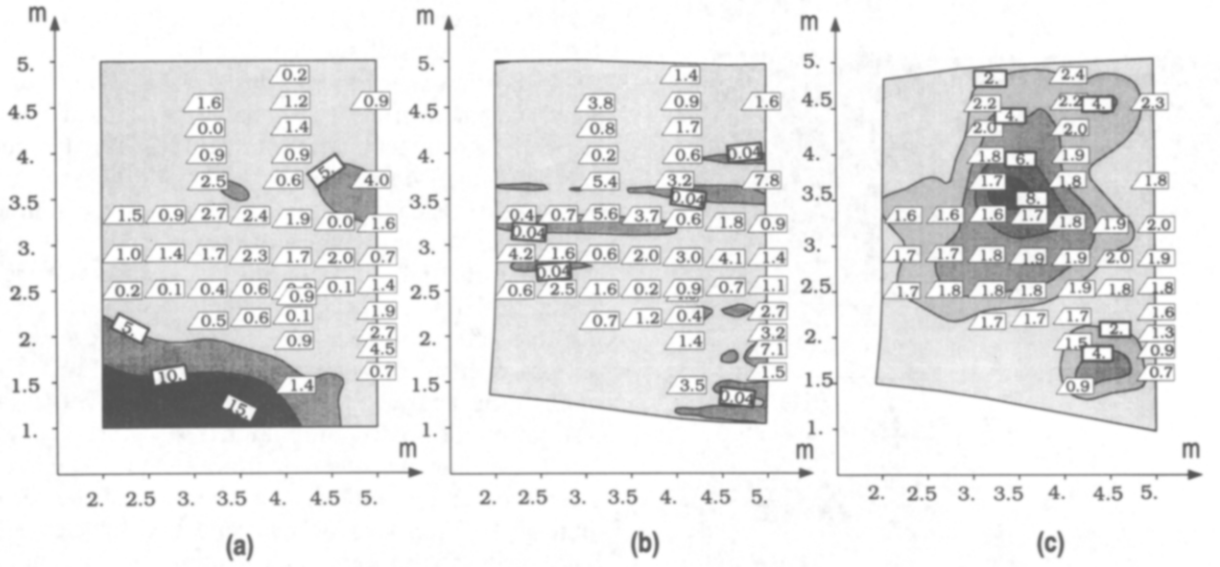

Fig. 6. RMS angle and distance for the approximation models of Fig. 5. The contour map indicates the distribution of the residual angle (digits in degrees in thick rectangular boxes) between the observed data and the fault surface model. The digits in the trapezoidal boxes indicate the distance (in centimetres along the y direction, see Figs. 3 and 4) between the observed data points and their equivalent in the fault surface model (the location of the points is indicated by the acute angle of the boxes). Figures 6(a–c) correspond respectively to the fault surfaces of Figs. 5(a–c).

geometrical characteristics of the well documented zone (zone with dense data).

For the fault model with thread criterion, the characteristics of the optimal twistor are such that the distance between each thread is 75 m. This large value compared to the size of the fault indicates that the slip is essentially a horizontal translation, with a very small rotation component. This is characteristic of strike-slip movement (which is by definition a true translation with zero rotation). The dashed lines in Fig. 5(b) represent the field lines of the twistor on the surface. These lines correspond to computed striae. These computed striae are well matched with the observed striae; the computed pitch is 10° whereas the observed pitch ranges from 9 to 11°.

As discussed above, the inverse problem may also be solved by fixing the coordinates of the twistor from the observed striae. When doing this (Figs. 5c and 6c) the result is not very different from the fault model obtained with an unknown twistor (Figs. 5b and 6b). However, it may be noted that when kinematic indicators (slip direction) are imposed (Fig. 6c), the RMS distances are better (1.7 cm), but the RMS angle values worse, than without such a constraint (Fig. 6b). Explanation may be expressed as follows: without an imposed slip direction, the modelled surface is as parallel as possible to the fault surface (but not necessarily near the surface), whereas the effect of an imposed slip direction leads to some local discrepancy in RMS angle but to a better mean proximity to the data.

The results for the fault B (see Fig. 3) are not discussed in detail here. The main results may be summarized as follows. Since this fault surface B is almost flat it is very close to the particular case of a flat surface with undetermined twistor direction. In this case, the use of the thread criterion does not significantly improve the geometry of the fault model and the computed striae may not be related to the observed striae. However, for such an almost-flat surface, the RMS distance and RMS angle values are very near to those obtained with an unknown twistor (Fig. 7b) if the striae measurements are imposed via twistor components, (see Fig. 7a).

Discussion

When using the thread criterion in the zone with dense data, very low RMS distance and RMS angle values are obtained. This indicates that the fault can be considered to be a thread surface. Two other results confirm this assumption: (i) when using thread criteria without a given twistor, the computed sliding displacement direction is very close to the measured striae and (ii) when using striae as fixed twistor coordinates, the fault model remains very close to the observed data.

In the zone with lack of data, the use of the thread criterion propagates information from the well documented areas (zones with dense data) to the poorly constrained areas and helps to establish the fault geometry in the latter. However, these results are obtained with a corrugated fault geometry. In the particular case of a near-flat surface, the use of the sliding direction as a fixed twistor is needed in order to get round the indetermination of the thread criterion associated with this type of surface.

APPLICATION TO THE SAN CAYETANO THRUST FAULT (CALIFORNIA)

The San Cayetano fault (Fig. 8a) is one of the major north-dipping thrusts in the northern part of the Ventura basin in the Transverse Ranges of California (Yeats 1983,

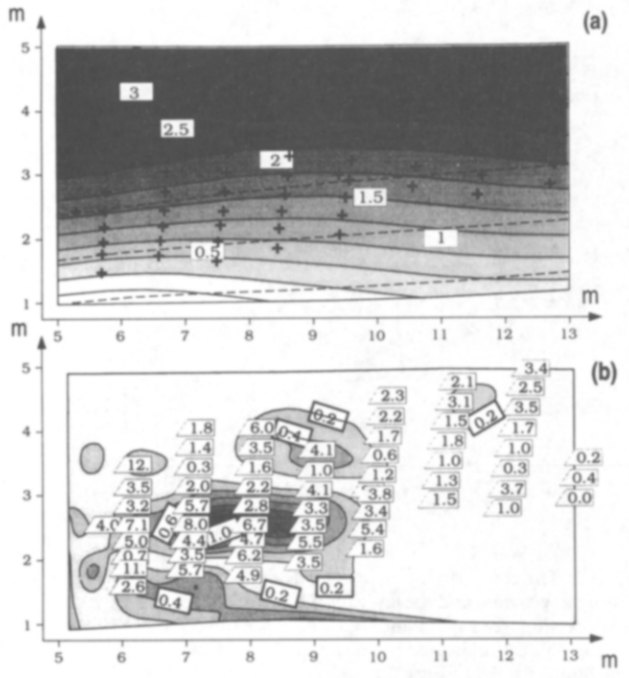

Fig. 7. (a) Approximation to one of the Cléry fault surfaces (referenced as B in Fig. 3), with the inverse method including approximation with proximity to data points, smoothness, thread criteria and the direction of striae measured on the outcrop. (b) RMS angle and distance for the approximation models in (a). The contour map indicates the distribution of the residual angles (digits in degrees in thick rectangular boxes) between the observed data and the fault surface model. The digits in the trapezoidal boxes indicate the distance (in cm along the y direction, see Figs. 3 and 4) between the observed data points and their equivalent in the fault surface models (the location of the points is indicated by the acute angle of the boxes). Crosses indicate the location of the surveyed data points on the fault surface. Dashed lines show the calculated twistor vector field.

Rockwell 1988, Çemen 1989, Hupfile 1991). This very recent thrust fault (0.5 Ma according to Yeats *et al.* 1994) accommodates the displacement of relatively rigid northern blocks (sandstone and shales) on to thick Quaternary and Pliocene sediment (Fig. 8b). Geological evidence, such as fold trend variations (110° to 070°) affecting recent sediments (less than 5 Ma), attests to a general 160° to 020° crustal shortening direction (Yeats *et al.* 1994). Earthquakes have occurred in the vicinity of the San Cayetano thrust, e.g. 1971 San Fernando earthquake along the north dipping Santa Susana fault (or some parallel fault). More recently, the south-dipping thrust fault (North Ridge fault) was active near the southern limit of the Ventura Basin. However, the deformation of the Ventura and neighbouring basins (Los Angeles, Santa Barbara Channel) is rather complex, with the possible effect of two block rotations revealed by paleomagnetism measurements (Luyendyk 1991), focal mechanism analysis (Jackson & Molnar 1990) and restoration of folded and faulted structures (Gratier 1993) revealing clockwise rotation of the whole Transverse Ranges and anticlockwise rotation of the eastern limit of the Transverse Ranges and Los Angeles basin. Since strike-slip movement is required in some models associated with the clockwise rotation, one regional question about the San Cayetano fault is whether this fault presents any evidence of horizontal displacement.

Data set: well data and outcrops

The Ventura basin contains oil-bearing formations, and hundreds of wells have been drilled through these formations. Of these wells, dozens penetrate the San Cayetano fault which is one of the best known faults. The opportunity was therefore taken to test the effect of the thread criterion on this fault. The available data were summarized by Hester & Truex (1977). In their report, the authors gave both the data (location of the wells and several cross-sections) and a unique fault surface obtained after interpolation of the entire data set (Fig. 9). However, since some authors (T. Hopps pers. comm.) propose that several fault surfaces may constitute the so-called San Cayetano fault, it was decided to treat the western and the eastern parts of the data set separately, Sespe creek being the separation line (see Fig. 9). The eastern part will be concentrated on here.

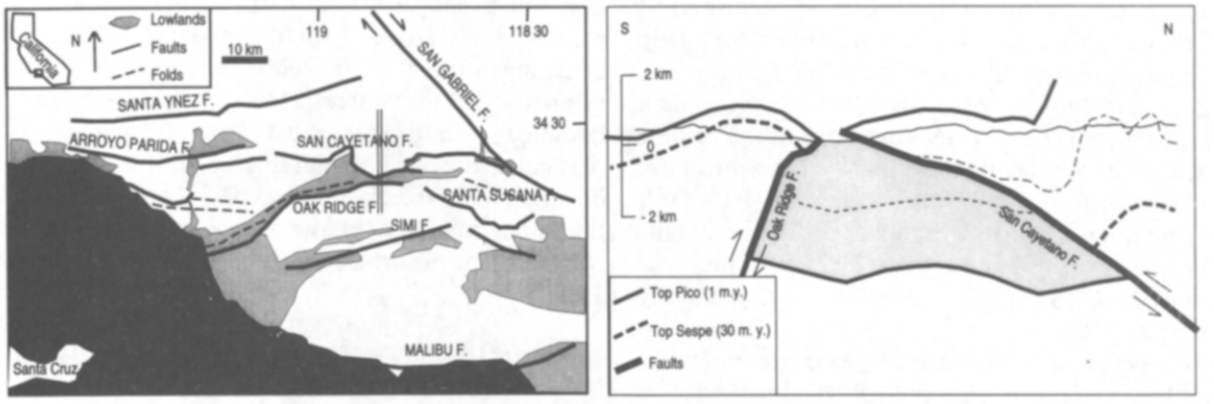

Fig. 8. Structural map of the Ventura basin (after Hupfile 1991) and cross-section through the San Cayetano thrust fault (after Yeats 1983). The thick line on the cross-section marks a horizon dated as 1 Ma old near Ventura and correlates east of this region. The projection of this horizon north of San Cayetano is highly speculative (Yeats 1983).

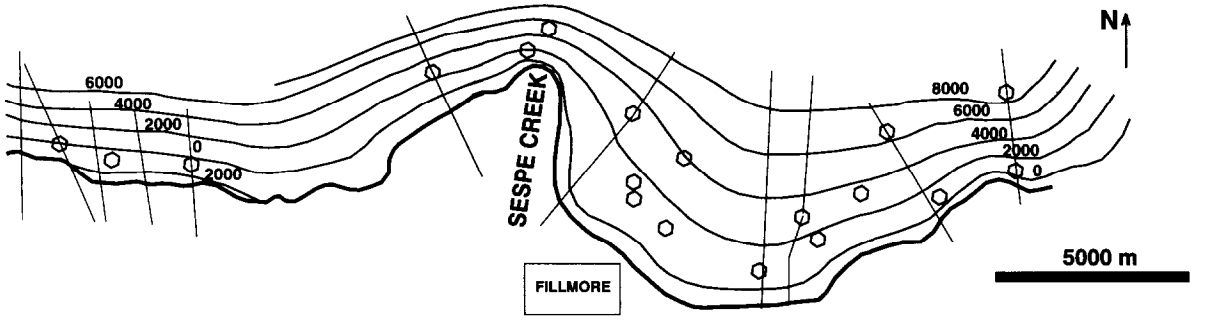

Fig. 9. Structure contour map of the San Cayetano fault surface from Hester & Truex (1977) with the location of wells (contour interval = 2000 ft) and the location of their original cross-sections (straight lines). The whole surface is partitioned between eastern (Figs. 10 and 11) and western parts (Fig.13) separated by Sespe Creek.

Results

The eastern part of the area comprises 13 wells and 5 outcrops which give the observed data set (18 observed data points) for the geometry of the fault surface.

A preliminary model was run without imposing any direction of displacement. The results are given in Figs. 10 and 11. In Fig. 10, the contoured values are the vertical elevation in km relative to a reference level at −3000 m; the vertical and horizontal axes are respectively the north and east directions. Crosses indicate the locations of the well and outcrop data for the fault surface. Figure 10(a) gives the results of the approximation without the thread criterion, whereas Fig. 10(b) gives the approximation with the thread criterion and an unknown twistor. Figures 11(a) and (b) give the RMS distance and angle values: the RMS distance values are given for each observed data point (trapezoidal boxes) whereas the RMS angles are given as contour maps (digits in thick rectangular boxes). As in the preceeding example, the two modelled surfaces are very close in the area of dense data whereas they differ in areas with sparse data. The RMS distance and angle values for the entire surface are almost the same for the two models (RMS distances 5.3 and 5.7 m, respectively without and with the thread criterion). With respect to the mean wavelength of the fault corrugation (about 10 km, see Fig. 10) the relative mean discrepancy is of the order of 0.05%. This shows that, in well documented areas, the fault surface is close to a thread surface.

In Fig. 10(b), the dashed lines indicate the computed striae direction. The mean orientation of these computed striae is 165°. This value is within the given range of the regional contraction direction (see discussion). A second type of model was run by imposing the twistor coordinate value. Since the characteristics of the striae at depth are obviously not known, the displacement direction was taken from the focal mechanisms of the neighbouring seismic thrust fault as 015° (Jackson & Molnar 1990). With this twistor value the modelled fault surface is given in Fig. 10(c). The fault surface is not very different from the previous one, the RMS distance for the whole surface being slightly higher at 10 m instead of 5.7 m, see Fig. 11(c). This shows that, for this fault, the use of the thread criterion (with and without the twistor orientation) can only constrain the direction of displacement within an uncertainty of 10–20°. However, the displacement must be associated with a thrust fault. Consequently, it also seems very unlikely that large strike-slip movements recently occurred on such a corrugated thrust fault.

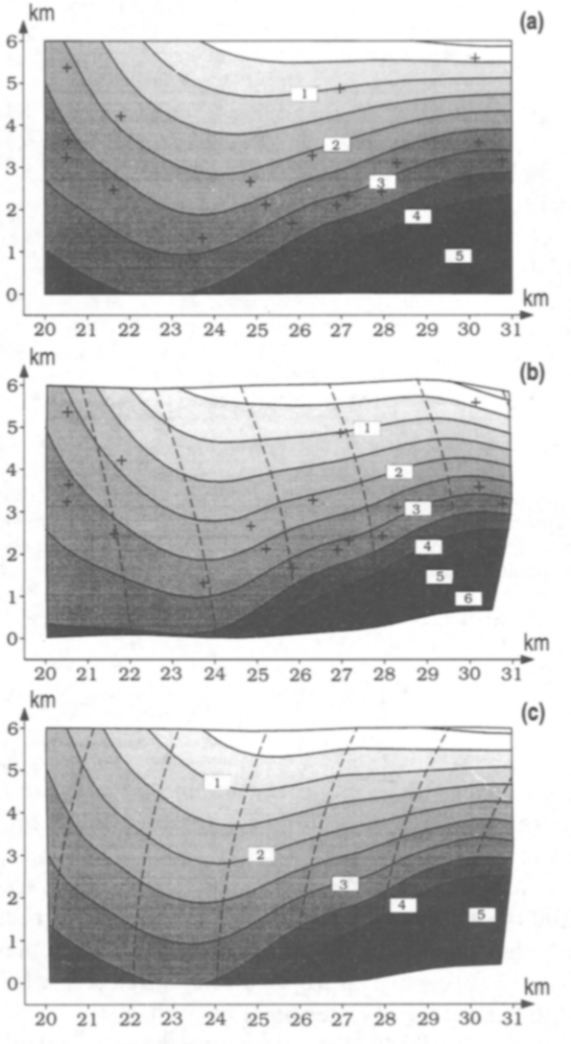

Fig. 10. Approximation of the eastern part of the San Cayetano fault surface (see Fig. 9), with the inverse method including various least-squares criteria. (a) Approximation with proximity to data points and smoothness criteria. (b) Approximation with proximity to data points, smoothness and thread criteria. (c) Approximation with proximity to data points, smoothness, thread criteria and imposed striae. The contoured values are the vertical elevation in km relative to a reference level at − 3000 m. The vertical and horizontal axes are respectively the north and east directions. Crosses indicate the location of the data on the fault surface: wells and outcrops. Dashed lines show the calculated twistor vector field.

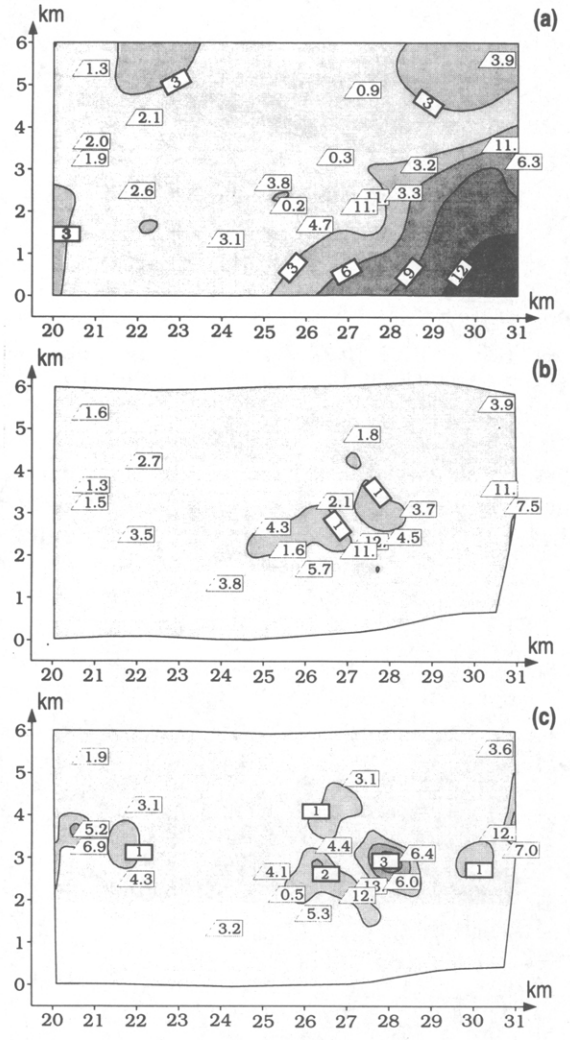

Fig. 11. RMS angle and distance for the approximation models of Fig. 10. The contour map indicates the distribution of the residual angles (digits in degrees in rectangular thick boxes) between the observed data and the fault surface model. The digits in the trapezoidal boxes indicate the distance (in m along the vertical elevation) between the observed data points and their equivalent in the fault surface models (the location of the points is indicated by the acute angle of the boxes); (a)–(c) correspond respectively to the fault surfaces of Figs. 10(a–c).

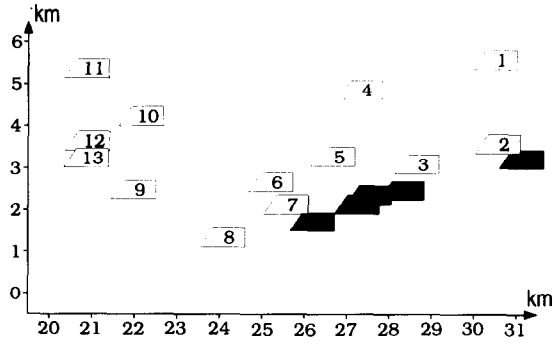

(a)

A	B	C
1	47.69	42.67
2	7.38	7.85
3	2.35	3.05
4	4.05	8.11
5	1.40	3.27
6	3.50	3.33
7	1.25	1.57
8	13.81	11.36
9	9.13	5.77
10	8.82	6.23
11	14.21	7.66
12	2.03	1.45
13	2.28	1.85

(b)

Fig. 12. Approximation of the eastern part of the San Cayetano fault surface. Blind tests on the 13 well data points. (a) Location and numbers of the wells used in the blind test. (b) Table of the results of these blind tests. A = number of the wells removed at each run, see (a); B = RMS distance (in m) between the observed data points and their equivalent in the fault models (for the entire surface = 12 wells) with proximity to data points and smoothness criteria; C = RMS distance (in m) between the observed data points and their equivalent in the fault models (for the entire surface = 12 wells) with proximity to data points, smoothness and thread criteria.

In order to test the effect of the thread criterion more accurately, blind tests were carried out. This common statistical method consists of successively removing one data item from the whole data set. The aim is to test the stability of the method when using the thread criterion. Only the 13 well data items were used for this calculation. Thus, 13 successive approximations were made with and without the thread criterion. For each of these approximations, the RMS distance between the observed and the computed data were estimated for the entire surface (for the 12 wells). The effect of each well is different (Fig. 12). When considering deviations of more than 1 m, the use of the thread criterion had a negative effect with only two wells (4 and 5). The thread criterion had a positive effect for five wells (1, 8, 9, 10 and 11). It is important to note the positive effect of the thread criterion for the wells which are near the boundaries of the studied area (1, 8 and 11). For the entire surface, the effect of the thread criterion is to decrease the mean distance between model and observation from 9 metres to 8 m (the fitting is improved by about 12%).

For the western part of the San Cayetano, only one result is given here (Fig. 13). In this part of the fault, a contour map of the fault surface was obtained by Hester & Truex (1977) with only three wells (located along the same elevation) and some cross-sections. When using random points taken from this map to determine the fault model, it was found that this fault is not far from a thread surface (Figs. 13 a & b), with a higher RMS distance (20–30 m) than for the eastern part. The value of the the computed striae direction is about 150°, slightly different from the eastern part of the fault (165°). However, the lack of data in this example could explain this uncertainty. This is shown when using the thread criterion with the same fixed twistor as for the eastern surface (015°, Fig. 13c). In this case, the RMS distance value did not significantly change. This example underlines the need for other wells to test this western part of the San Cayetano fault surface as a thread surface.

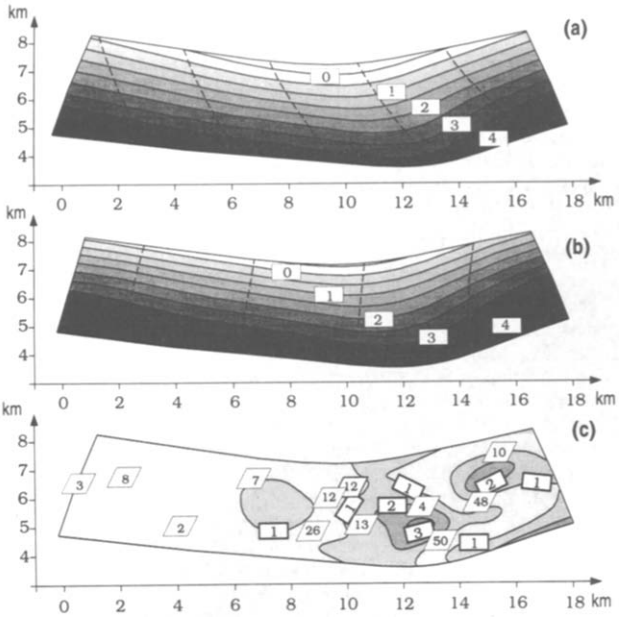

Fig. 13. Approximation of the western part of the San Cayetano fault surface (see Fig. 9), with the inverse method including various least-squares criteria. (a) Approximation with proximity to data points, smoothness, thread criteria. (b) Approximation with proximity to data points, smoothness, thread criteria and the direction of displacement estimated from seismic focal mechanisms. Dashed lines show the calculated twistor vector field. (c) RMS angle and distance for the approximation models of the Fig. 13(b). The contour map indicates the distribution of the residual angles (digits in degrees in rectangular thick boxes) between the observed data and the fault surface model. The digits in the trapezoidal boxes indicate the distance (in m) between the observed data points and their equivalent in the fault surface models (the location of the points is indicated by the acute angle of the boxes).

Discussion

Some results concerning the San Cayetano thrust fault are very similar to those of the Vercors strike-slip fault, and are summarized in the conclusion as follows: with dense data sets, thrust faults like the San Cayetano fault are very nearly thread surfaces. Other results come from the use of particular techniques. Blind tests on the well data set show that RMS distances are lower with the thread criterion than without the thread criterion particularly for wells near the boundaries of the studied area. When using the thread criterion, the computed striae direction is found to be 165°. Slip directions in this region are known from three types of data: seismic focal mechanisms of neighbouring thrust faults indicate a 010–020° direction (Jackson & Molnar 1990), space geodetic measurements indicate a 160–170° direction (Feigl *et al.* 1993) and computational restoration of folded and faulted strata (Gratier 1995) gives a 000–010° direction. When using the thread criterion with fixed twistor components (015°), the fault surface remains a possible thread surface. These results show that the San Cayetano fault has a main thrust displacement. The possible shortening direction associated with this thrust displacement is compatible with the shortening direction of the Transverse Ranges given in the literature (160° to 200°).

CONCLUSIONS

In order to obtain the best possible fault geometry approximation, an inverse method has been developed to study the effect of several criteria: proximity to data points, smoothness and thread criteria. This latter criterion is based on the assumption that large relative displacements of jointed solid blocks define a thread surface. Most often, one of the blocks is more rigid than the other and this induces small to large corrugations.

In order to test the effect of the various criteria, several models were made either using only the proximity to data points and the smoothness criteria or including the thread criterion. When using the thread criterion there are two possibilities: either compute the striation on the fault (which can be compared with natural markers of this displacement such as striae or focal mechanisms); or use information from natural markers as approximation parameters. Root mean square values (RMS, both in distance and angle) are used to estimate the discrepancy between observed (geological) data and computed data.

Two corrugated faults with dense data points have been used as examples. Despite differences between the two: (i) in the mean wavelength value of the corrugation (5 m and 10 km respectively), (ii) in the type of fault (strike-slip and thrust fault respectively) and (iii) in the nature of the faulted rocks (limestone and sandstone/shale formations respectively), very similar results are obtained. In both cases, the observed data fit very well with a thread surface. In both cases, the discrepancy (RMS distance) between fault model and observed data remains lower than the accuracy of the data. In both cases, the use of the thread criterion allows the entire surface to be controlled by the geometric characteristics of the best documented zone. When using the thread criterion in order to estimate the direction of fault displacement the results fit well with the displacement direction (estimated either with direct measurements of the fault striae or by comparison with seismic focal mechanisms, geodetic data or computational restoration).

With a flat surface, the use of the sliding direction as a fixed twistor is needed in order to get round the indetermination of the thread criterion associated with this type of surface.

From a general point of view the assumption that jointed solid blocks slipping against each other define a thread surface between them is well supported. These properties can thus be used in the proposed inverse method to best define the geometry of faults when these faults are only described by scattered data.

Acknowledgements—We wish to thank T. Barr, R. Norris and an anonymous referee for their helpful reviews. MT was supported by a grant from the Ministère de l'Éducation Nationale (France). We are particularly indebted to Charles M. Marle (Paris VI University) for his idea of characterizing threads by the parallelism to some twistor and to Tom Hopps and John Crowell for their help to characterize the San Cayetano fault. This work was also partially supported by the Commission of the European Communities (DG XII, contract No. JOU2-CT92-0099).

REFERENCES

Arnaud, H. 1981. De la plate-forme urgonienne au bassin vocontinen: le Barrémo–Bédoulien des Alpes occidentales entre Isère et Buech (Vercors méridional, Diois oriental, Dévoluy). Unpublished PhD thesis, Université Joseph Fourier, Grenoble, France.

Barr, D. 1985. 3D palinspastic restoration of normal faults in the Inner Moray Firth: implication for extensional basin development. *Earth Planet. Sci. Lett.* **75**, 191–203.

Bartels, R. H., Beatty, J. C. & Barsky, B. A. 1987. *Introduction to splines for use in computer graphics and geometric modeling*. Morgan Kaufman Publishers Inc., California.

Bennis, C., Vézien, J. M. & Iglesias, G. 1991. Piecewise surface flattening for non-distorted texture mapping. *Comput. Graphics* **25**, 237–246.

Çemen, I. 1989. Near surface expression of the eastern part of the San Cayetano fault: a potential active thrust fault in the California Transverse Ranges. *J. geophys. Res.* **94**, 9665–9677.

Chamberlin, R. T. 1910. The Appalachian folds of Central Pennsylvania. *J. Geol.* **18**, 228–251.

Cobbold, P. R. 1979. Removal of finite deformation using strain trajectories. *J. Struct. Geol.* **1**, 67–72.

Dahlstrom, C. D. A. 1969. Balanced cross-sections. *Can. J. Earth Sci.* **6**, 743–757.

Feigl, K. L., Agnew, D. C., Bock, Y., Dong, D., Donnellan, A., Hager, B. H., Herring, T. A., Jackson, D. D., Jordan, T. H., King, R. W., Larsen, S., Larson, K. M., Murray, M. H., Shen, Z. & Webb, F. H. 1993. Space geodetic measurements of crustal deformation in central and southern California, 1984–1992. *J. geophys. Res.* **98**, 21677–21712.

Goguel, J. 1952. *Traité de Tectonique*. Masson, Paris.

Gratier, J. P. 1993. Partition between seismic and aseismic deformation in California. Unpublished Southern California Earthquake Center report.

Gratier J. P. 1995. Displacement field and geometric compatibility using computational restoration of folded and faulted strata: application to the last 3–4 Ma in the Ventura and Los Angeles basin, *AGU abstract*, San Francisco.

Gratier, J. P. & Guillier, B. 1993. Compatibility constraints on folded and faulted strata and calculation of the total displacement using computational restoration (UNFOLD program). *J. Struct. Geol.* **15**, 391–402.

Gratier, J. P., Guillier, B., Delorme, A. & Odonne, F. 1991. Restoration and balance of a folded and faulted surface by best-fitting of finite elements: principle and applications. *J. Struct. Geol.* **13**, 111–115.

Gratier, J. P., Ménard G. & Arpin, A. 1989. Strain–displacement compatibility and restoration of the Chaînes Subalpines of the Western Alps. In *Alpine Tectonics* (edited by Coward, M. P., Dietrich, D. & Park, R. G.). *Spec. Publs. geol. Soc. Lond.*, 65–81.

Hester, R. L. & Truex, J. N. 1977. San Cayetano fault field trip, AAPG Pacific section.

Hossack, J. R. 1979. The use of balanced cross-sections in the calculation of orogenic contraction, a review. *J. geol. Soc. Lond.* **136**, 705–711.

Hupfile, G. J. 1991. Thin skinned tectonics of the Upper Ojai Valley and Sulphur Mountain area, Ventura basin, California. *Am. Ass. Petrol. Geol. Bull.* **75**, 1353–1373.

Jackson, J. & Molnar, P. 1990. Active faults and block rotation in the Western Transverse Ranges. *J. geophys. Res.* **95**, 22073–22087.

Kerr, H. G., White, N. & Brun, J. P. 1993. An automatic method for determining three-dimensional normal fault geometries. *J. geophys. Res.* **98**, 17837–17857.

Léger, M., Morvan, J. M. & Rakotoarisoa, H. 1995. Inversion of 3D geological structures using parallelism, developability and smoothness least-squares criteria. *Geophys. J. Intern.* **121**, 63–81.

Léger, M., Morvan, J. M. & Thibaut, M. in press. Least-squares optimization of fault surfaces using the rigid blocks approximation. *Geophys. J. Intl.*

Lisle, R. J. 1992. Constant bed-length folding: three-dimensional geometric implications. *J. Struct. Geol.* **14**, 245–252.

Luyendyk, B. P. 1991. A model for Neogene crustal rotations, transtension and transpression in southern California. *Geol. Soc. Am. Bull.* **103**, 1528–1536.

McCoss, A. M. 1988. Restoration of transpression/transtension by generating the three-dimensional segmented helical loci of deformed lines across structure contour maps. *J. Struct. Geol.* **10**, 109–120.

Rakotoarisoa, H. 1992. Modelisation geometrique et optimisation de structures geologiques 3D. Unpublished PhD Thesis, Specialite: Mathématiques, Univrtdité Claude Bernard-Lyon I, Technip, Paris.

Robert, J. P. 1976. Étude de la fracturation aux abords des décrochements des massifs subalpins dauphinois. Unpublished PhD Thesis, Université Joseph Fourier, Grenoble, France.

Rockwell, T. 1988. Neotectonics of the San Cayetano fault Transverse Ranges, California. *Geol. Soc. Am. Bull.* **100**, 500–513.

Rouby, D., Cobbold, P. R., Szatmari, P., Demercian, S., Coelho, D. & Rici, V. A. 1993. Least-squares palinspastic restoration of regions of normal faulting, Application to the Campos basin (Brasil). *Tectonophysics* **221**, 439–452.

Rougée, P. 1982.*Mécanique Générale*. Edition Vuibert Université, Paris.

Schumaker, L. L. 1981. *Spline Functions: Basic Theory*. John Wiley and Sons, New York.

Suppe, J. 1983. Geometry and kinematics of fault-bend folding. *Am. J. Sci.* **283**, 648–721.

Tarantola, A. 1987. *Inverse problem theory*. Elsevier, Amsterdam.

Thibaut, M. 1994. Géométrie des surfaces de faille et dépliage 3D, méthodes et applications. Unpublished PhD Thesis, Université Joseph Fourier, Grenoble, France.

Yeats, R. S. 1983. Large scale Quaternary detachment in Ventura basin, southern California. *J. geophys. Res.* **88**, 569–583.

Yeats, R. S., Hupfile, G. J. & Stitt, L. T. 1994. Late Cenozoic tectonics of the East Ventura basin, Transverse Ranges, California. *Am. Ass. Petrol. Geol. Bull.* **78**, 1040–1074.